Effects of Pulsation to the Mean Field and Vortex Development in a Backward-Facing Step Flow

Sharul S. Dol[1,2]
e-mail: sharulsham@curtin.edu.my

M. Mehdi Salek

Robert J. Martinuzzi

Department of Mechanical
and Manufacturing Engineering
University of Calgary
Calgary, Alberta, T2N 1N4 Canada

This work is concerned with the behavior of pulsatile flows over a backward-facing step geometry. The paper mainly focuses on the effects of the pulsation frequency on the vortex development of a 2:1 backward-facing step for mean Reynolds number of 100 and for $0.035 \leq St \leq 2.19$. The dependence of the flow field on the Reynolds number ($Re = 100$ and 200) was also examined for a constant Strouhal number, St of 1. A literature survey was carried out and it was found that the pulsation modifies the behavior of the flow pattern compared to the steady flow. It was shown in the present work that the inlet pulsation generally leads to differences in the mean flow compared to the steady field although the inlet bulk velocity is the same due to energy redistribution of the large-scale vortices, which result in nonlinear effects. The particle-image velocimetry results show that the formation of coherent structures, dynamical shedding, and transport procedure are very sensitive to the level of pulsation frequencies. For low and moderate inlet frequencies, $0.4 \leq St \leq 1$, strong vortices are formed and these vortices are periodically advected downstream in an alternate pattern. For very low inlet frequency, $St = 0.035$, stronger vortices are generated due to an extended formation time, however, the slow formation process causes the forming vortices to decay before shedding can happen. For high inlet frequencies, $St \geq 2.19$, primary vortex is weak while no secondary vortex is formed. Flow downstream of the expansion recovers quickly. For $Re = 200$, the pattern of vortex formation is similar to $Re = 100$. However, the primary and secondary vortices decay more slowly and the vortices remain stronger for $Re = 200$. The strength and structure of the vortical regions depends highly on St, but Re effects are not negligible. [DOI: 10.1115/1.4025608]

Keywords: backward-facing step, pulsatile flow, Reynolds stress, vortex shedding

1 Introduction

The internal separated flow regions such as in the backward-facing step (BFS) appear in many engineering and biomedical applications. Examples of these include flows in heat exchangers or through sudden expansions in pipe networks. A BFS is also a suitable prototypical example for regions of flow recirculation-reattachment in physiological flows, such as in arterial bifurcation, stenoses, and many biomedical devices, including venous and urinary catheters, fluid transfer implants, and artificial heart valves [1]. In these kinds of applications, the inlet flows are normally pulsatile and often characterized by zones of highly unstable and disturbed flows downstream of the step.

The flow over a BFS with steady inlet condition has been extensively studied both experimentally and numerically [2–8]. Armaly et al. [2] reported that the length of the recirculating flow region in the immediate vicinity of the BFS (primary vortex) has strong, nonlinear dependence on the Reynolds number (Re). An upper wall recirculation region (secondary vortex) appears for $Re > \sim 400$ due to the adverse pressure gradient created by the sudden expansion. The flow field downstream the step becomes unsteady due to the complex interaction between these vortices [8].

For lower Reynolds number, such that the flow remains laminar, the flow is relatively well understood for steady inlet conditions. However, for unsteady or pulsatile inlet conditions, the flow inside a BFS remains poorly explored. Pulsatility is a major characteristic of physiological flows and gives rise to physical complexity such as inducing unsteady flow separation and transient wall shear stresses. Haidekker et al. [9] in their experimental study of the BFS as an *in vitro* model to examine the response of mammalian cells to spatial and temporal wall shear stress variations showed that under pulsatile conditions, the BFS geometry causes local amplification of the shear stress in the recirculation region and that strong temporal gradients of the of flow also leads to a significant stimulation of endothelial cell growth.

A BFS with pulsating inlet flow is expected to be more prone to vortex formation and shedding at much lower Reynolds number than the steady flow [10–12]. Valencia and Hinojosa [13] showed that pulsatile flows lead to an early breakdown of the primary recirculation region and the generation of upper wall instability. Rani et al. [8] observed a roof vortex instability but at $Re \sim 1500$ (for steady inlet velocity). Rosenfeld [12] numerically studied the pulsating flow behind a constricted channel at $45 < Re < 1500$ for various forcing dimensionless frequencies St and he found that the moving vortices are generated even for Reynolds number as small as 90. At low pulsation Strouhal number, strong vortices develop through the roll-up of shear layers and shedding is regular. As the Strouhal number increases, the vortices are observed to decrease in intensity. The underlying mechanism is still not well understood but is expected to be related to the formation time since results show that the strength and structure of the vortical regions depend on the period of the pulsation. Rosenfeld [12] also only discussed the flow physics qualitatively. The effects of forcing pulsation period to the formation of both primary and secondary vortices, vortex propagation, interactions, and decay are still poorly understood.

The flow fields depend primarily on four parameters: (i) the Reynolds number, $Re = U_0 D/\nu$ where U_0 is the average bulk velocity upstream of the BFS, D is the hydraulic diameter of the

[1]Corresponding author.
[2]Present address: Department of Mechanical Engineering, Curtin University, Sarawak Campus CDT 250, 98009 Miri, Sarawak, Malaysia

Contributed by the Fluids Engineering Division of ASME for publication in the JOURNAL OF FLUIDS ENGINEERING. Manuscript received June 3, 2013; final manuscript received September 30, 2013; published online October 18, 2013. Assoc. Editor: Mark F. Tachie.

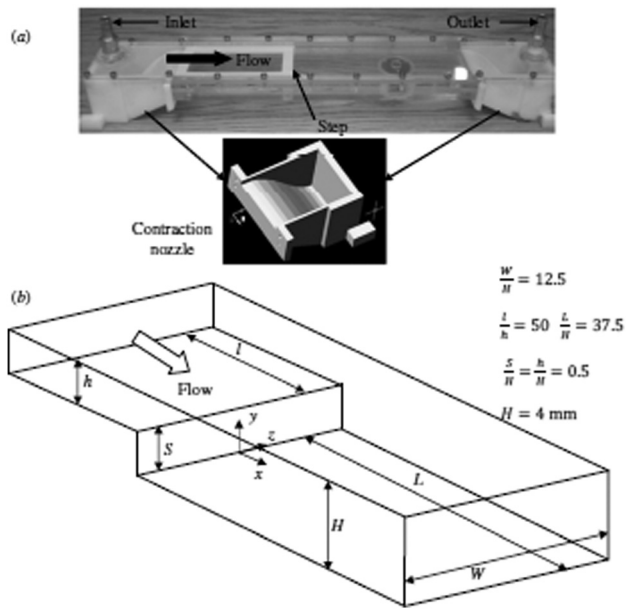

Fig. 1 BFS channel; (*a*) photograph of the channel; (*b*) schematic of the BFS

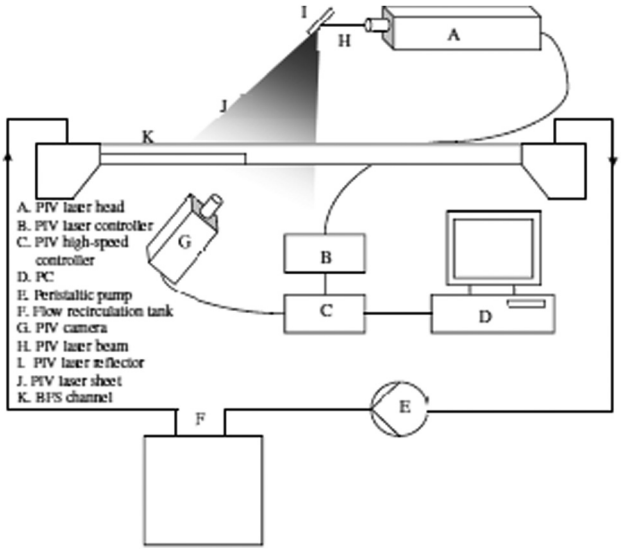

Fig. 2 A schematic of the experimental setup

inlet channel, and ν is the kinematic viscosity of the fluid; (ii) the pulsation Strouhal number, $St = fD/U_0$ where f is the pulsation frequency; (iii) the pulsation amplitude A; and (iv) the BFS expansion ratio, $ER = H/h$ where H and h are, respectively, the downstream and upstream channel heights. Only the first two parameters will be considered here. The third parameter has been investigated by [14,15] while the fourth parameter, which is normally related to three-dimensional effects, has been thoroughly studied by Ref. [6] for a steady inlet condition.

The objectives of the present work are: first to show that the mean characteristics of the pulsatile flow is different from the steady flow for the same Re; and second to investigate the effects of the pulsation St and Re on the laminar yet unsteady flow field downstream of the BFS. For the influence of St, the phase-averaged velocity fields obtained by high-frame-rate particle image velocimetry (PIV) are analyzed at an average $Re = 100$ and for $0.035 \leq St \leq 2.19$. The discussions will center on the vortex formation and evolution. For the influence of the Reynolds number, the PIV data for $Re = 200$ and for $St = 1$ are added to the discussion.

2 Experimental Apparatus and Techniques

The flow considered in this paper was investigated by means of high-frame-rate particle image velocimeter. The experimental investigation was performed in the BFS water channel as shown in Fig. 1(*a*). This is a closed-loop flow chamber with a 250-mm long working section. It incorporates backward-facing step with an expansion ratio (H/h) of 2.0. The flow enters through a nozzle with an area contraction ratio of 10:1. The outlet of the nozzle is connected to the inlet of the channel test section, which is 2 mm in height (h), 50 mm in width (W), and 100 mm in length up to the backward-facing step (l). These dimensions ensure a two-dimensional fully developed flow at the cross section where the step is located. The downstream length (L) to the outlet of the channel is 150 mm. This BFS model has an aspect ratio of $W/h = 25$, which is sufficient to eliminate three-dimensional wall effects in the center of the span [16]. A schematic of the BFS is shown in Fig. 1(*b*).

The experimental setup is schematically shown in Fig. 2. The flow pulsation was generated by a Masterflex L/S variable speed peristaltic pump (model number: 7524-40) by Cole-Parmer. The pump has a four cams or rollers assembly with an adjustable speed range of 10 to 600 rpm. The speed can be regulated at ± 1 rpm resolution. The Reynolds number used in this study is defined based on $2h$ (hydraulic diameter of the inlet channel) and average bulk velocity upstream of the channel U_0.

Flow field information was obtained by using a LaVision FlowMaster high-frame-rate PIV system. The ability of the system to simultaneously give very high spatial resolution velocimetry over a relatively large flow region and time resolved flow fields make the technique essential to the study of evolving dynamics of coherent structures. Silicon-carbide particles with 8 μm nominal diameter were added to the water and used as tracers. The flow was illuminated by double-pulsed Nd:YLF laser (Photonics Industries DM20-527, $\lambda = 527$ nm) with a maximum energy of 20 mJ per pulse per laser head at a repetition rate of 1000 Hz.

In the present study the image recoding unit is a digital high-speed 10-bit CMOS camera of type HighSpeedStar 5 with maximum frame rate of 250 kHz. It has resolution of 1024×1024 pixels, captured at 3 kHz frame rates and the pixel size is $17\ \mu\text{m} \times 17\ \mu\text{m}$. The camera was fitted with an AF micro-Nikkor 60 mm f/2.8D lens and the object distance was adjusted to obtain a field-of-view of $\sim 18.4 \times 18.4$ mm^2. The spatial resolution was 0.0179856 mm/pixel. Single-frame mode with recording rate of 125–1000 Hz was used and 500–1000 frames per acquisition were recorded in all the experiments. The vector analysis was done via DaVis 7.2 software in two steps: multipass with decreasingly smaller sizes interrogation windows of 64×64 and 16×16 pixel were used in the first and second step, respectively, to achieve more precise results and higher spatial resolution. An overlap of 50% of the interrogation area was used together with a Gaussian window function to minimize the loss of pairs. A detailed description of the technique and the uncertainty estimation can be found in [17].

2.1 Vortex Identification. This work mainly aims to explain formation and evolutionary dynamics of coherent structures and to explore the role of coherent structures in pulsatile flow. However, to establish their dynamical significance, coherent structure properties must be determined. The criterion for vortex identification proposed by Ref. [18], known as the λ_2-criterion, was used. In this method, vortex boundaries are defined as regions of negative values of the second eigenvalue of the symmetric tensor $S^2 + \Omega^2$ where S and Ω are, respectively, the symmetric and antisymmetric portions of the velocity gradient tensor ∇u. These authors define a vortex core as a "connected region with two negative eigenvalues of $S^2 + \Omega^2$." This method is a suitable criterion

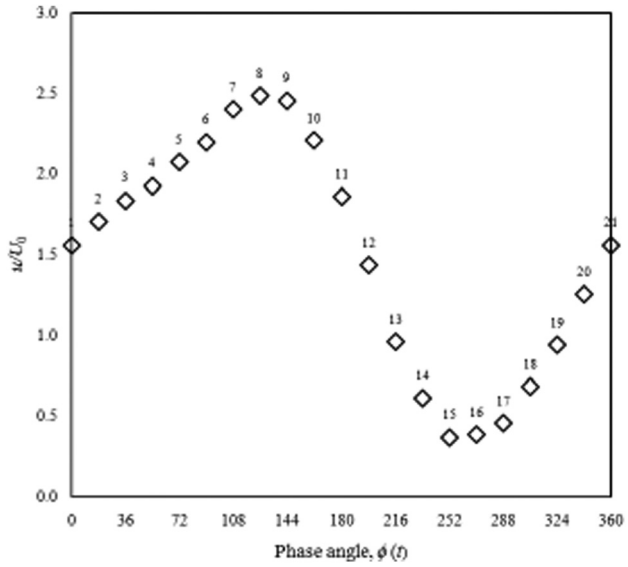

Fig. 3 Phase-averaged velocity in a pulsation cycle for $St = 0.4$ ($Re = 100$). The streamwise velocity profiles are at the channel centerline upstream the BFS. The numbers refer to the phase values $\phi_n, n = 1, \ldots .20$ with $\Delta\phi = 18$ deg.

especially for unsteady and low Reynolds number, wall-bounded flow where the background shear is comparable to the vorticity magnitude within the vortex.

2.2 Phase-Averaged Velocities. In order to have a consistent phase reference for all PIV vector fields, local maxima of the flow pulsation was detected from the PIV velocity time series data. For the double decomposition ensemble averaging, the flow pulsation period was discretized into 20 phases steps $\phi_n, n = 1, \ldots .20$. The phase $\phi(t) \in [0, 360\,\text{deg}]$ was then determined with $\Delta\phi = 18$ deg. The ensemble average was undertaken for each phase step such that any PIV data points within $\pm\Delta\phi/2$ was used for the discrete phase. Figure 3 shows an example of the phase value for the pulsatile flow ($Re = 100$ and $St = 0.4$) captured at rates of 250 Hz for 4 s or approximately 80 data points per pulsation period over 12 cycles of flow pulsation were calculated for the statistics.

3 Results and Discussions

3.1 Mean Flows. The main objective for this section is to highlight the main differences between flow fields arising from laminar pulsatile and steady inlet flow conditions. The present approach is to show that the mean of the pulsatile and the steady flow fields are different. This would imply nonlinear interactions reflected in the momentum equation (e.g., fluctuating stresses), which could then be related to differences in the vortex dynamics. To help in the analysis, it is helpful to separate the pulsatile flow field in mean and cyclical (or coherent) fluctuating components. The instantaneous steady momentum equation in Cartesian tensor notation is given as

$$u_j \frac{\partial u_i}{\partial x_j} = -\frac{1}{\rho_0}\frac{\partial p}{\partial x_i} + \nu \frac{\partial^2 u_i}{\partial x_j \partial x_j} \tag{1}$$

The instantaneous physical variables are decomposed into their mean part (U, V, and P) and a deviation from the mean, the fluctuating coherent component (u_c, v_c, and p_c). The mean of the momentum equation then takes the form

$$U_j \frac{\partial U_i}{\partial x_j} + \frac{\partial}{\partial x_j}(\overline{u_{ci}u_{cj}}) = -\frac{1}{\rho_0}\frac{\partial P}{\partial x_i} + \nu \frac{\partial^2 U_i}{\partial x_j \partial x_j} \tag{2}$$

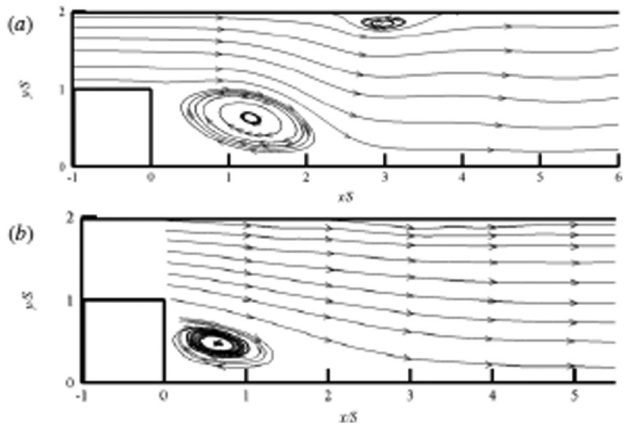

Fig. 4 Mean streamlines patterns ($Re = 100$); (*a*) $St = 0.4$; (*b*) steady case

The terms $-\rho_0\overline{u_{ci}u_{cj}}$ are analogous to an additional stress (Reynolds stress) exerted by the velocity fluctuations (due to flow pulsation) on the mean flow. Basically, the normal stresses $\overline{u_c^2}$ and $\overline{v_c^2}$ need to be spatially invariant and the shear stress $\overline{u_c v_c} = 0$ for the mean of the pulsatile flow field to be identical to the steady flow field.

The mean streamlines patterns for $St = 0.4$ ($Re = 100$) is shown in Fig. 4(*a*). The velocity distributions for the steady flow field have been thoroughly discussed in Refs. [2,17]. The inlet pulsation leads to different flow behavior downstream of the sudden expansion compared to the steady flow field (Fig. 4(*b*)). The main different between the mean flow for the pulsatile and steady cases is the appearance of the upper wall recirculation region (secondary vortex). This upper wall separation only happens at $Re > \sim 400$ for the steady case. The upper wall vortex leads to a destabilization in the flow field through concave curvature instability of the boundary layer [8,19] and, thus, it is expected the circulation will be shed.

Although the average Reynolds number for $St = 0.4$ is the same to the steady case ($Re = 100$), the mean velocity profiles show differences, as shown in Fig. 5. The streamwise velocity profile at $x/S = 1$ (Fig. 5(*a*)) shows that the flow inside the primary recirculation region (backflow) has higher velocity magnitude, implying the vortex has greater circulation for the pulsatile case. The streamwise velocity profile at $x/S = 5$ for the steady flow shows that the velocity fields are close to that of a fully developed channel (parabolic profile) while the flow is still redeveloping for the pulsatile case (Fig. 5(*b*)). The transverse velocity profiles also indicate the deviations from the steady flow behavior (Fig. 5(*c*)). These differences can be attributed to modification to the momentum transfer due to the flow pulsatility.

Contours of Reynolds stresses, $\overline{u_c^2}$, $\overline{v_c^2}$, and $-\overline{u_c v_c}$ normalized by U_0^2 are shown in Fig. 6 for $St = 0.4$. The Reynolds normal stress $\overline{u_c^2}$ shows peak intensity in the regions of strong velocity gradients $\partial u/\partial y$, particularly in the separated shear layer close to the step and the upper wall vortex vicinity. The distribution of $\overline{v_c^2}$ is characterized by one extended peak area, which matches the formation region of the primary vortex. The Reynolds stress $\overline{v_c^2}$ distribution is not monotonic. Local maxima are observed downstream of the recirculation zone. As will be discussed in the next section, this behavior is related to the vortex dynamics. The Reynolds shear stress $-\overline{u_c v_c}$ distribution shows peaks in the regions of strong velocity gradient $\partial u/\partial y$ and is related to the fluctuating kinetic energy contents in the vortex structures. Clearly, these results show that the $\overline{u_c^2}$ and $\overline{v_c^2}$ are not spatially invariant and the fluctuations are anisotropic ($\overline{u_c^2} \neq \overline{v_c^2}, \overline{u_c v_c} = 0$). Hence, the structures arising during pulsatile flow give rise to nonlinear behavior, affecting momentum transfer in the mean.

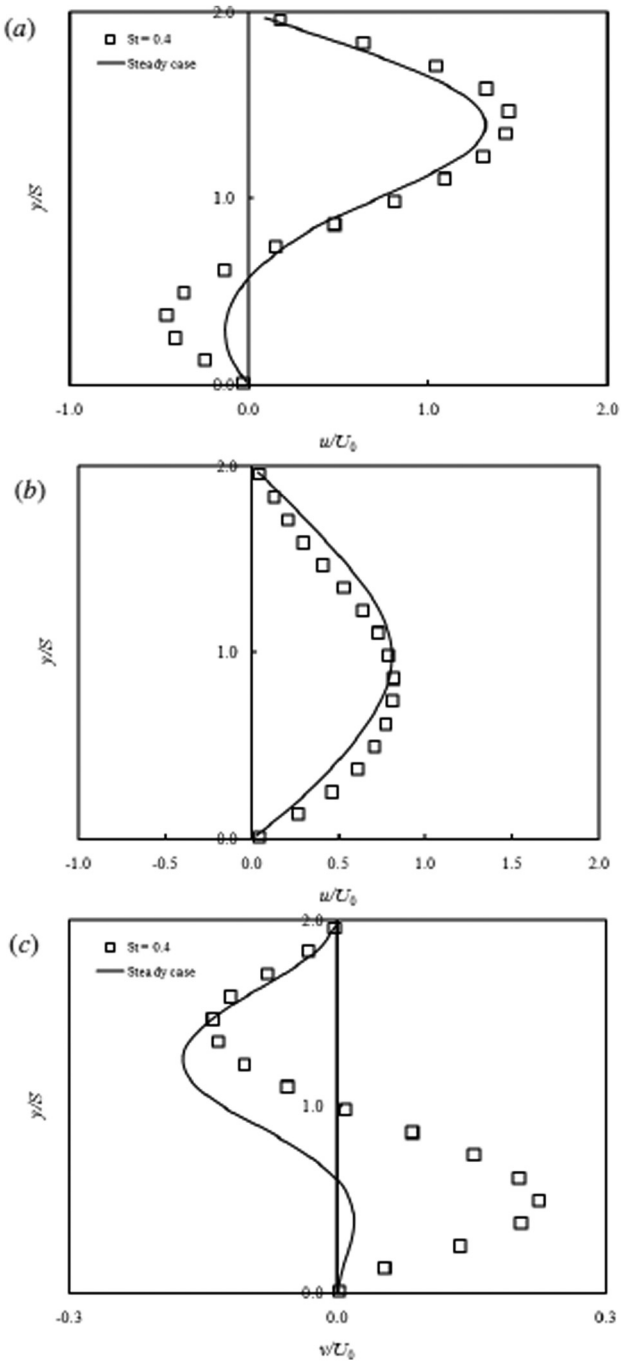

Fig. 5 Mean velocity profiles for $Re = 100$; (*a*) streamwise, $x/S = 1$; (*b*) streamwise, $x/S = 5$; (*c*) transverse, $x/S = 1$

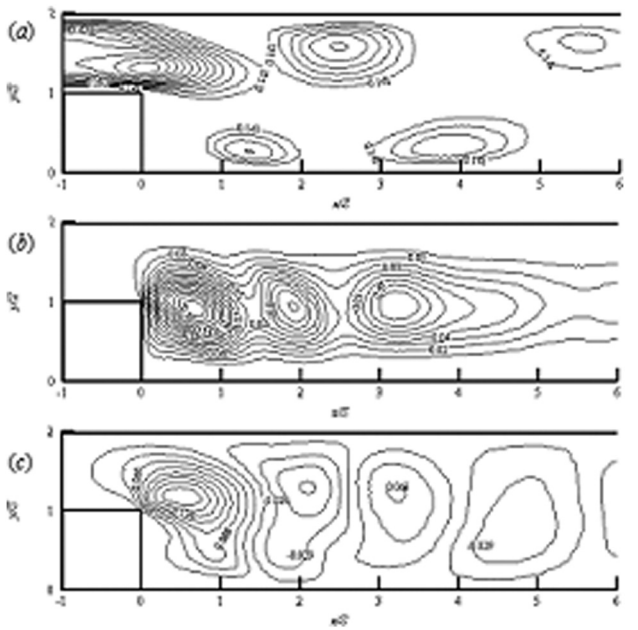

Fig. 6 Reynolds stress contours for $St = 0.4$ ($Re = 100$); (*a*) $\overline{u_c^2}/U_0^2$; (*b*) $\overline{v_c^2}/U_0^2$; (*c*) $-\overline{u_2 v_2}/U_0^2$

3.2 Influence of Strouhal Number, $0.035 < St < 2.19$. The difference in the physics seen in the mean flow suggests that the instantaneous (phase-averaged) fields are affected by the flow pulsations. Figure 7 shows the formation and advection of vortices identified with $\lambda_2 < 0$ contours for $St = 1$ at different phases in a pulsation cycle while Fig. 8 of the phase-averaged vorticity $\langle\omega\rangle = \partial\langle v\rangle/\partial x - \partial\langle u\rangle/\partial y$ contour plots at selected phases. Together, these figures illustrate the vortex evolution. Following the notation of Ref. [12], the primary and secondary vortices in Fig. 7 are, respectively, labeled by P_n and S_n, where n is an index that refers to the generation of these vortices relative to the present cycle n. The formation of primary and secondary vortices in a pulsation cycle and their alternate advection downstream are apparent. The primary vortex originates at the edge of the step ($x/S = 0$). The flow pulsation amplifies the Kelvin–Helmholtz instability causing the shear layer to roll-up forming a primary recirculation region that contains clockwise (negative) vorticity behind the step. The primary vortex grows in strength (Fig. 7(*a*)–7(*f*)) as it is fed with vorticity from the separated shear layer (Fig. 8(*a*)–8(*c*)) during the formation process until the vortex reaches its maximum circulation (at the end of the deceleration phase).

The primary vortex is forced to detach due to the appearance of counterclockwise (positive) vorticity near the wall at this instant (at the minimum flow rate, as shown in Fig. 8(*d*)) when the flow close to the wall changes sign. The supply of circulation to the vortex has been interrupted due to this opposite-sign vorticity, the vortex detaches and is convected from the formation region by the mean flow during the acceleration phase. The vortex rapidly loses strength upon leaving the formation area.

The formation process of the secondary vortex is different from that of the primary. The formation and shedding of the primary vortex induces an upper wall flow separation. The growing primary vortex interacts with the upper wall flow by inducing an additional deceleration ($\partial u/\partial x < 0$) superimposed on that due to the sudden expansion effect resulting in a larger adverse pressure gradient along the upper wall. The secondary vortex reaches its maximum circulation upon shedding exactly one cycle after the initial formation, which is triggered by the passage of the primary vortex. It travels down and passes over the secondary vortex causing it to pinch-off. The region between P_n and S_n coincides with the location of a local maximum in $\overline{v_c^2}$. Weaker local maxima are also observed at locations between downstream vortex pairs (during intervals of low advective speed) due to the rotating motion of the vortices.

These coherent structures are very sensitive to the level of pulsation frequencies. The results for $St = 0.4$ ($Re = 100$) show that the pattern of vortex formation and evolution is similar to $St = 1$ but the generated primary and secondary vortices are stronger for the former case. Figure 9 shows the rms of the transverse velocity at $y/S = 1$ (channel centerline) and the results suggest that the wake region for $St = 0.4$ is characterized by stronger vortical activity. The vortex is strong enough to increase the persistence of the dynamical coupling between shed vortices, which is essential in perseverance of alternating rows of vortices downstream the step. These primary and secondary vortices form a trail of strong

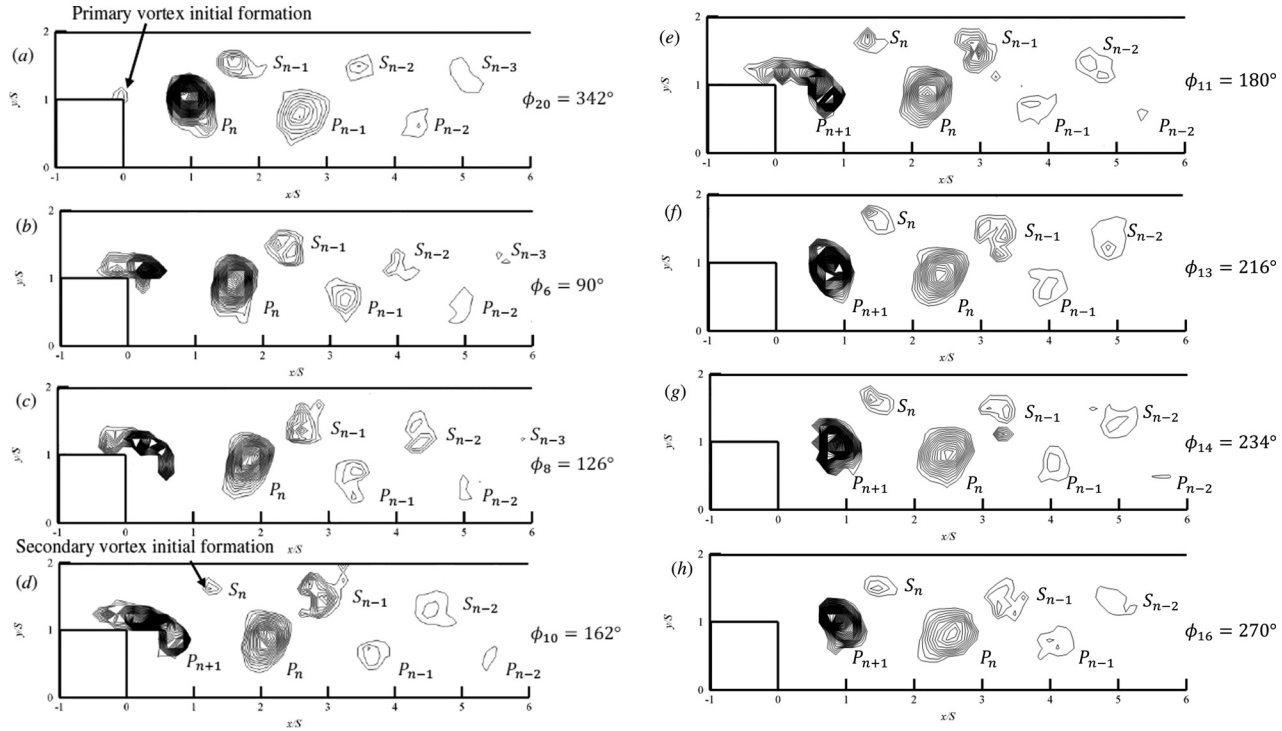

Fig. 7 Contour plot of λ_2-criterion for $St = 1$ ($Re = 100$); (*a*) $\phi_{20}(t) = 342$ deg; (*b*) $\phi_6(t) = 90$ deg; (*c*) $\phi_8(t) = 126$ deg; (*d*) $\phi_{10}(t) = 162$ deg; (*e*) $\phi_{11}(t) = 180$ deg; (*f*) $\phi_{13}(t) = 216$ deg; (*g*) $\phi_{14}(t) = 234$ deg; (*h*) $\phi_{16}(t) = 270$ deg

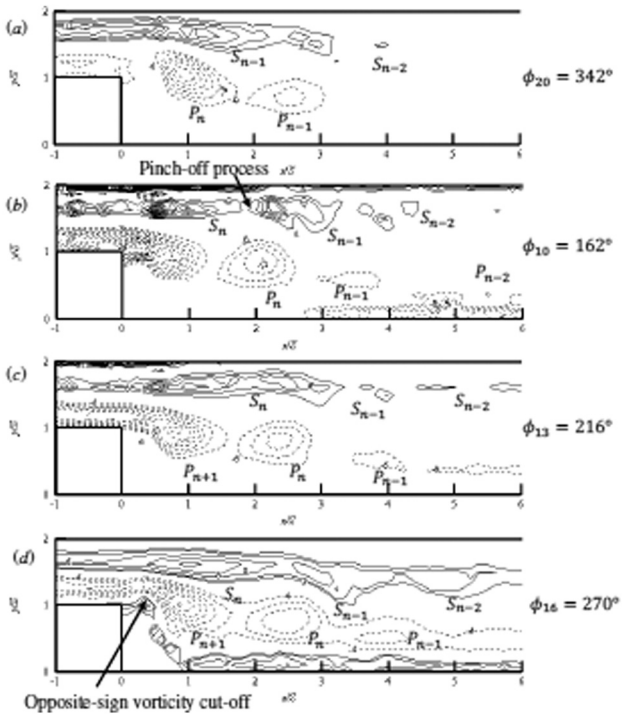

Fig. 8 Phase-averaged vorticity contours for $St = 1$ ($Re = 100$) at different ϕ_n; (*a*) $\phi_{20}(t) = 342$ deg; (*b*) $\phi_{10}(t) = 162$ deg; (*c*) $\phi_{13}(t) = 216$ deg; (*d*) $\phi_{16}(t) = 270$ deg. Dashed (solid) lines represent constant negative (positive) normalized vorticity values $\langle\omega\rangle D/U_0$.

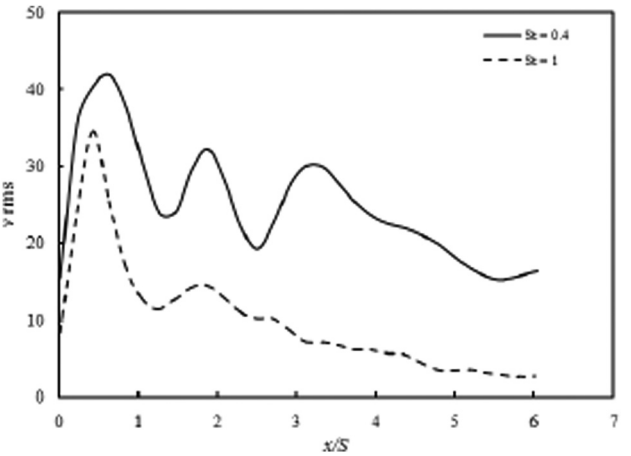

Fig. 9 Plots of *v* rms $\left[\left(\overline{v^2}\right)^{1/2}/U_0\right]$ at $y/S = 1$

convective vortices, resulting in a highly oscillating flow field. Since the initial circulation is significantly larger for $St = 0.4$, allowing the vortices to persist further downstream than for $St = 1$.

For $St = 0.035$, the formation of primary and secondary vortices is regular but no shedding is observed. Although the forming primary and secondary vortices are much stronger (e.g., compared to $St = 0.4$), these remain bound during the cycle and both the primary and secondary vortices lose their strength as soon as they enter the deceleration phase and eventually disappeared at the end of the pulsation cycle. Pulsatile flow with very small Strouhal number behaves more like a steady flow [15,20].

For $St = 2.19$ case, the primary vortices are much smaller in size and weaker with no upper wall vortices are formed. The shed primary vortex is weak, suggesting that the induced deceleration at the upper wall is insufficient to cause boundary layer separation. Hence, the trail of vortices of alternate sign cannot form. The flow downstream of the step resembles a fully developed pulsatile channel flow (time derivative of the velocity is balanced by the pressure gradient).

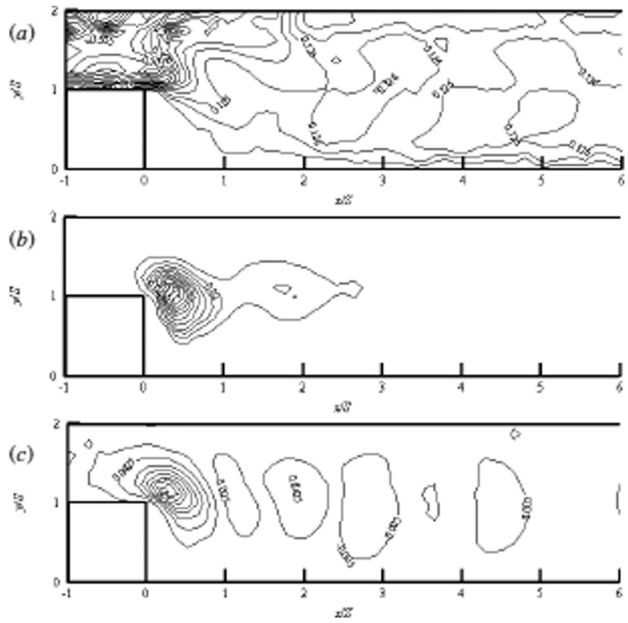

Fig. 10 Reynolds stress contours for $St = 1$ ($Re = 100$); (*a*) $\overline{u_2^2}/U_0^2$; (*b*) $\overline{v_2^2}/U_0^2$; (*c*) $-\overline{u_2 v_2}/U_0^2$

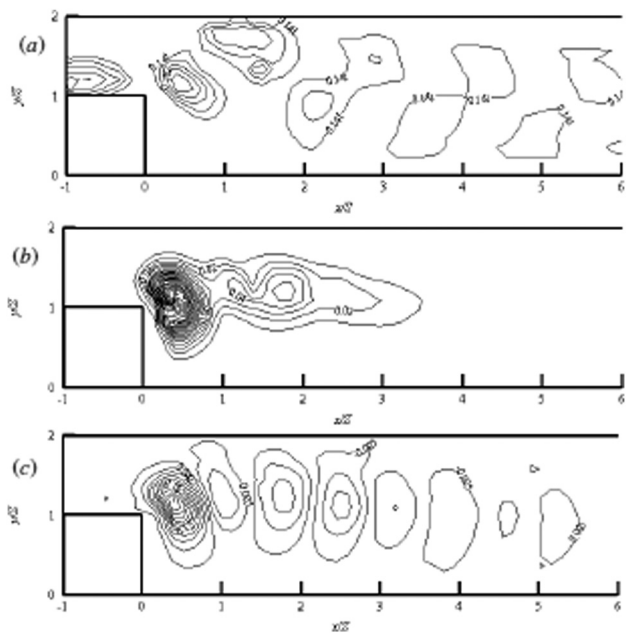

Fig. 11 Reynolds stress contours for $St = 1$ ($Re = 200$); (*a*) $\overline{u_2^2}/U_0^2$; (*b*) $\overline{v_2^2}/U_0^2$; (*c*) $-\overline{u_2 v_2}/U_0^2$

3.3 Influence of Reynolds Number, $Re = 100$ and 200. The dependence of the flow field on the Reynolds number was studied for a constant Strouhal number of 1. The results show qualitative similarity when compared to the results for the same St and for $Re = 100$. The distribution of the Reynolds stresses suggests that the mean flow fields in both cases are governed by similar size of flow structures, vortex arrangements, and interactions (Figs. 10 and 11). The main difference between $Re = 100$ and 200 is the primary vortex gets slightly stronger for the latter case and the vortices survive longer. At $Re = 200$, the primary and secondary vortices decay more slowly, indicating a possibility of dissipation or mixing scales differently.

4 Conclusion

The mean of the pulsatile flow was shown to differ from the steady flow although the inlet bulk velocity is the same. An upper wall vortex, in the mean, was generated at much smaller Reynolds number for the pulsatile flow than in the steady case that resulted in different flow behavior downstream the sudden expansion. The Reynolds stress distributions in the pulsatile flow suggested the flow was dominated by nonlinear interactions of large-scale vortices, which the strength and structures were influenced by the pulsation Strouhal number and Reynolds number. While they exist, the primary and secondary vortices are advected downstream in an alternate pattern with the shedding frequency locks on to the flow pulsation frequency.

Acknowledgment

Sharul S. Dol would like to acknowledge Talisman Energy Inc. for the Talisman Energy Graduate Scholarship in Energy & Related Studies. Thanks are also due to the NSERC Research Facility and Discovery Grant Program.

References

[1] Truskey, G. A., Barber, K. M., Robey, T. C., Olivier, L. A., and Combs, M. P., 1995, "Characterization of a Sudden Expansion Flow Chamber to Study the Response of Endothelium to Flow Recirculation," ASME J. Biomech. Eng., **117**(2), pp. 203–210.
[2] Armaly, B. F., Durst, F., Pereira, J. C. F., and Schönung, B., 1983, "Experimental and Theoretical Investigation of Backward-Facing Step Flow," J. Fluid Mech., **127**, pp. 473–496.
[3] Grant, I., Owens, E., and Yan, Y., 1992, "Particle Image Velocimetry Measurements of the Separated Flow Behind a Rearward Facing Step," Exp. Fluids, **12**, pp. 238–244.
[4] Williams, P. T., and Baker, A. J., 1997, "Numerical Simulations of Laminar Flow Over a 3D Backward-Facing Step," Int. J. Num. Meth. Fluid., **24**, pp. 1159–1183.
[5] Kostas, J., Soria, J., and Chong, M. S., 2002, "Particle Image Velocimetry Measurements of a Backward-Facing Step Flow," Exp. Fluids, **33**(6), pp. 838–853.
[6] Biswas, G., Breuer, M., and Durst, F., 2004, "Backward-Facing Step Flows for Various Expansion Ratios at Low and Moderate Reynolds Numbers," ASME J. Fluids Eng., **126**(3), pp. 362–374.
[7] Schram, C., Rambaud, P., and Riethmuller, M. L., 2004, "Wavelet Based Eddy Structure Education From a Backward Facing Step Flow Investigated Using Particle Image Velocimetry," Exps. Fluids, **36**, pp. 233–245.
[8] Rani, H. P., Tony, W. H. S., and Eric, S. F. T., 2007, "Eddy Structures in a Transitional Backward-Facing Step Flow," J. Fluid Mech., **588**, pp. 43–58
[9] Haidekker, M. A., White, C. R., and Frangos J. A., 2001, "Analysis of Temporal Shear Stress Gradients During the Onset Phase of Flow Over a Backward-Facing Step," ASME J. Biomech. Eng., **123**, pp. 455–463.
[10] Sobey, I. J., 1985, "Observation of Waves During Oscillatory Channel Flow," J. Fluid Mech. **151**, pp. 395–426.
[11] Tutty, O. R., 1992, "Pulsatile Flow in a Constricted Channel," ASME J. Biomech. Eng., **114**(1), pp. 50–54.
[12] Rosenfeld, M., 1995, "A Numerical Study of Pulsating Flow Behind a Constriction," J. Fluid Mech., **301**, pp. 203–223.
[13] Valencia, A., and Hinojosa, L., 1997, "Numerical Solutions of Pulsating Flow and Heat Transfer Characteristics in a Channel With a Backward-facing Step," Heat Mass Transf., **32**, pp. 143–148.
[14] Cohen, J. M., 1995, "Transient Flow Over a Backward-Facing Step," Ph.D. thesis, University of Connecticut, Storrs, CT.
[15] Salek, M. M., Dol, S. S., and Martinuzzi, R. J., 2009, "Analysis of Pulsatile Flow in a Separated Flow Region," Proc. ASME 2009 Fluids Engineering Division Summer Meeting FEDSM2009, Vail, CO.
[16] de Brederode, V., and Bradshaw, P., 1972, "Three-Dimensional Flow in Nominally Two-Dimensional Separation Bubbles, I. Flow Behind a Rearward-Facing Step," Imperial College of Science and Technology, London, Aero Report 72-19.
[17] Dol, S. S., 2011, "Particle Image Velocimetry Investigation of Pulsatile Flow over a Backward-facing Step," Ph.D. thesis, University of Calgary, Calgary, Alberta, Canada.
[18] Jeong, J., and Hussain, F., 1994, "On the Identification of a Vortex," J. Fluid Mech. **285**, pp. 69–94.
[19] Ghia, K. N., Osswald, G. A., and Ghia, U., 1989, "Analysis of Incompressible Massively Separated Viscous Flows Using Unsteady Navier–Stokes equations," Int. J. Num. Meth. Fluid., **9**, pp. 1025–1050.
[20] Zamir, M., 2000, *The Physics of Pulsatile Flow*, Springer, New York.